Environmental Research 210 (2022) 112749

Contents lists available at ScienceDirect

Environmental Research

journal homepage: www.elsevier.com/locate/envres

Inactivation behavior and intracellular changes in *Escherichia coli* during electro-oxidation process using Ti/Sb–SnO_2/PbO_2 anode: Elucidation of the disinfection mechanism

Sasikaladevi Rathinavelu [a,b,1], Govindaraj Divyapriya [a,1], Angel Joseph [a], Indumathi M. Nambi [a,*], Anantha Barathi Muthukrishnan [b], Guhan Jayaraman [b]

[a] Environmental and Water Resources Division, Department of Civil Engineering, Indian Institute of Technology Madras, Chennai, Tamil Nadu, 600 036, India
[b] Department of Biotechnology, Bhupat and Jyoti Mehta School of Biosciences, Indian Institute of Technology Madras, Chennai, Tamil Nadu, 600 036, India

ARTICLE INFO

Keywords:
Electro-oxidation
ROS
Disinfection
Escherichia coli
•OH radical
Mechanism

ABSTRACT

This study investigates the behavior and intracellular changes in *Escherichia coli* (model organism) during electro-oxidation with Ti/Sb–SnO_2/PbO_2 anode in a chlorine free electrochemical system. Preliminary studies were conducted to understand the effect of initial *E. coli* concentration and applied current density on disinfection. At an applied current density 30 mA cm^{-2}, 7 log reduction of *E. coli* was achieved in 75 min. The role of reactive oxygen species' (ROS) in *E.coli* disinfection was evaluated, which confirmed hydroxyl (•OH) radical as the predominant ROS in electro-oxidation. Observations were carried out at cell and molecular level to understand *E. coli* inactivation mechanism. Scanning electron microscopy images confirmed oxidative damage of the cell wall and irreversible cell death. Intracellular and extracellular protein quantification and genetic material release further confirmed cell component leakage due to cell wall rupture and degradation due to •OH radical interaction. Change in cell membrane potential suggests the colloidal nature of *E. coli* cells under applied current density. Plasmid deoxyribonucleic acid degradation study confirmed fragmentation and degradation of released genetic material. Overall, effective disinfection could be achieved by electro-oxidation, which ensures effective inactivation and prevents regrowth of *E. coli*. Disinfection of real wastewater was achieved in 12 min at an applied current density 30 mA cm^{-2}. Real wastewater study further confirmed that effective disinfection is possible with a low cost electrode material such as Ti/Sb–SnO_2/PbO_2. Energy consumed during disinfection was determined to be 4.978 kWh m^{-3} for real wastewater disinfection at applied current density 30 mA cm^{-2}. Cost of operation was estimated and stability of the electrode was studied to evaluate the feasibility of large scale operation. Relatively low energy and less disinfection time makes this technology suitable for field scale applications.

1. Introduction

Disinfection plays a crucial role in determining the quality of drinking water and treated wastewater. Conventional and large-scale wastewater treatment technologies such as chlorination, ultraviolet (UV) irradiation, ozonation and solar treatment have been employed for disinfection for several years now (Jin et al., 2019). However, the widely adopted disinfection process is the chlorination. Chlorination though cost-effective suffers from limitations such as formation of carcinogenic intermediates viz; chloro-organics and chloramines, presence of residual chlorine, unpleasant taste, failure to inactivate certain group of bacteria and inability to prevent regrowth in the absence of residual chlorine (Dan et al., 2013; Jin et al., 2019; C. Zhang et al., 2021).

In recent times, advanced oxidation processes (AOP) such as electro-Fenton, electro-peroxi coagulation, electro-coagulation, pulsed power technology, photocatalysis, etc., have been widely studied for disinfection of water and wastewater (Foster et al., 2011; Kourdali et al., 2018; Singh et al., 2016). Electro-oxidation process (EOP) is one such AOP, which is a promising disinfection process and offer several advantages viz; ease of installation, operation and maintenance, effective

* Corresponding author.
E-mail address: indunambi@iitm.ac.in (I.M. Nambi).
[1] These authors have contributed equally.

https://doi.org/10.1016/j.envres.2022.112749
Received 21 August 2021; Received in revised form 15 December 2021; Accepted 14 January 2022
Available online 3 February 2022

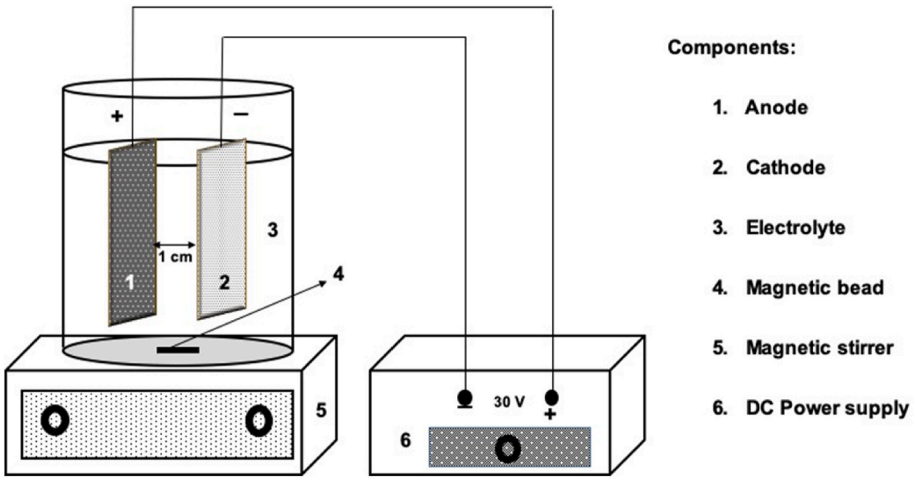

Fig. 1. Illustration of the electro-oxidation experimental setup.

disinfection of wide array of bacteria, and less land requirement (Long et al., 2015). EOP is a heterogeneous process, where electric potential is applied across electrodes and •OH radicals are generated when water is discharged at the anode (Eq. (1)) (Cuerda-Correa et al., 2020).

$$M + H_2O \rightarrow M(\bullet OH) + H^+ + e^- \quad (1)$$

M (•OH) denotes physisorbed hydroxyl radical on the anode (M) surface.

In EOP, the anode material and generated ROS determines the efficiency of disinfection. Anodes can be briefly classified into *active* anodes and *non-active* anodes. In case of *active* anodes, •OH radicals generated strongly interact with the anode surface and becomes chemisorbed. The chemisorbed •OH radicals at the anode surface participate in direct oxidation of pollutants. Thus, the oxidation of pollutants at the surface of *active* anodes are incomplete and results in transformation of pollutants. Platinum electrodes, mixed metal oxide electrodes and dimensionally stable electrodes namely iridium oxide and ruthenium oxide are *active* anodes (Jiang et al., 2021; Rajasekhar et al., 2021). In case of *non-active* anodes, •OH radicals are weakly bound and are physisorbed at the anode surface. Physisorbed •OH radicals are readily available for interaction with the pollutants resulting in complete mineralization. Examples of *non-active* anodes include boron-doped diamond (BDD), lead oxide (PbO_2) and tin oxide (SnO_2) (Rajasekhar et al., 2020, 2021). Widely studied *non-active* anode for *E. coli* disinfection by EOP is BDD (Bruguera-Casamada et al., 2016; Lacasa et al., 2013; Li et al., 2010; Long et al., 2015; Thostenson et al., 2018) *Non-active* anode such as BDD can effectively disinfect water and wastewater. However, the cost of electrode fabrication is high, which makes it unsuitable for large scale applications (Rajasekhar et al., 2020). One of the cost effective and *non-active* is PbO_2 with an oxygen over potential of 1.6–

2.0 V/SHE (Elaissaoui et al., 2019; Martínez-Huitle et al., 2015; Panizza and Cerisola, 2009; Rajasekhar et al., 2020). PbO_2 electrode is equally efficient as BDD but cost effective due to easy fabrication and has comparatively long service time (Xia et al., 2019).

Electrooxidation of pollutants such as azo dyes (Acid Orange 7, Acid Red G), persistent organic pollutants (para-aminophenol, perfluorocarboxylic acid, bisphennol-A), inorganic compound (hydrazine), surfactants (perfluorooctanoic acid), pesticide (nitenpyram), herbicide (linuron), alkanes and PAHs using PbO_2 electrodes are previously reported (Abu Ghalwa et al., 2016; Lin et al., 2012; Rajasekhar et al., 2021; Weng and Yu, 2019; Xia et al., 2019; Xue et al., 2011; Yang et al., 2020; Yuan et al., 2019). However, papers on disinfection using PbO_2 are limited. Furthermore, these studies have demonstrated only the ability of PbO_2 in disinfecting *E. coli*, *Enterococcus faecalis*, total coliforms and fecal coliforms. S. Chen et al. (2016) studied the disinfection efficiency of graphite felt/PbO_2 on synthetic ballast water containing *E. coli*, and *Enterococcus faecalis*. On the other hand, Rahmani et al. (2019) evaluated the effect of operating parameters such as electrolyte concentration, applied current density, pH, electrode material (stainless steel/PbO_2 and lead/PbO_2) and total dissolved solids on disinfection efficiency in synthetic wastewater containing total coliform and fecal coliform. However, effectiveness of the EOP disinfection to prevent the regrowth of bacteria using PbO_2 is not evaluated.

In microorganisms, the cell wall protects the cell organelles and maintains cell integrity. Cell proteins, enzymes, and genetic material play an important role in cell metabolism and survival. Reported disinfection studies suggest that predominant *E. coli* (model organism) death/inactivation in an EOP is due to oxidative damage of cell membrane and cell components due to ROS interaction (Giannakis et al., 2018; Long et al., 2015). However, knowledge on how the *E. coli* cells behave during EOP disinfection, changes in cell wall potential and cell size, extent of cell wall damage, protein, and genetic material release and degradation of cell organelles are also limited. It is important to assess and understand the extent of damage due to EOP in *E. coli* in order to evaluate the effectiveness of disinfection. Moreover, in the recent times attention is being given to chloride free electrooxidation based disinfection methods to avoid the formation of disinfection by products (Bakheet et al., 2018; Bruguera-Casamada et al., 2016; Isidro et al., 2020; Long et al., 2015). To the best of our knowledge mechanism of *E. coli* inactivation by EOP using PbO_2 in a chlorine free media is not proposed. Since the process is energy driven, it is also important to estimate the cost of operation, evaluate and compare the energy efficiency of the process with other state of art technologies for scale up and operation.

Therefore, the objectives of this study are i) to evaluate a low-cost PbO_2 anode for effective disinfection of *E. coli* in a chlorine free media ii) to elucidate the intracellular changes that occur during disinfection, iii) to propose a mechanism for *E. coli* inactivation and iv) to determine the energy consumed during EOP disinfection. In this study, the effect of applied current density and initial *E. coli* concentration were studied. Effectiveness of disinfection was evaluated by performing regrowth studies. Role of different ROS in EOP disinfection process was studied and the predominant ROS was identified. To understand the morphology changes, scanning electron microscopy (SEM) analysis is performed. Change in intracellular adenosine triphosphate (ATP), dry cell weight, intracellular protein concentration, genetic material concentration, zeta potential, cell size, and functional group due to oxidative damage were observed and recorded to understand the intracellular changes that occur during disinfection. Non-specific interaction of •OH radicals with the cells were confirmed by Fourier-transform infrared spectroscopy (FTIR) analysis. To evaluate the disinfection efficiency,

energy efficiency and feasibility of real-time application, disinfection of real wastewater was performed, energy consumed for disinfection was determined, cost of operation was estimated energy was estimated and compared with other disinfection technologies and stability of the electrode was evaluated.

2. Materials and methods

2.1. Electrode preparation and characterization

Ti/Sb–SnO_2/PbO_2 anode used in this study was prepared in the laboratory with titanium plate (Sigma-Aldrich, India) as substrate. Initially, titanium substrate was prepared and dip coated with Sb–SnO_2 as described by (Rajasekhar et al., 2020). PbO_2 was electrochemically deposited on both sides of the intermediate layer Sb–SnO_2 (Hao et al., 2015). For coating the PbO_2 layer, the reaction was carried out in a 250 mL electrochemical cell placed in a water bath maintained at 60 ± 5 °C at an applied current density 30 mA cm^{-2}. Stainless steel electrode was used as the cathode. Surface morphology and energy dispersive X-ray analysis of the synthesized electrode were performed with FEI Quanta FEG 200-High Resolution Scanning Electron Microscope (Fig. S1). A detailed study on electrode characterization is published by our research group (Rajasekhar et al., 2020).

2.2. Experiment setup

The reaction was set up with Ti/Sb–SnO_2/PbO_2 anode and a stainless cathode separated by a distance of 1 cm in a single compartment cell with an active surface area of 3 × 2 cm^2 on each side of the electrode and connected to a DC power supply (Fig. 1). The reaction volume was 150 mL with 25 mM of sodium sulfate (Na_2SO_4) (Merck, India) as the electrolyte and stirred continuously with a magnetic stirrer at rpm 150 ± 20. A single colony of *E. coli* (model organism) was inoculated in 3 mL nutrient broth (Himedia, India). 3 mL culture was incubated at 37 °C in an orbital shaker for 3 h and was then transferred to 97 mL of nutrient broth. 100 mL was incubated overnight at 37 °C in an orbital shaker (150 rpm). 20 mL of this overnight culture was taken, centrifuged (5000 rpm) for 5 min. The obtained pellet was re-suspended in 150 mL of 25 mM Na_2SO_4 and was used for all the experiments (~10^7 CFU mL^{-1} *E. coli* cells). To study the effect of initial cell concentration, 10 mL of the overnight culture was taken, and centrifuged (5000 rpm) for 5 min and resuspended in 150 mL of 25 mM Na_2SO_4. To study the effect of applied current density, experiments were carried out at different applied current density 10, 20, and 30 mA cm^{-2}. Subsequent experiments were carried out at an applied current density 30 mA cm^{-2} unless mentioned otherwise. For the plasmid degradation study, 50 mL reaction volume containing plasmid pPROTet of ~3 ng μL^{-1} concentration in 25 mM Na_2SO_4 was used. Samples before and after degradation were subjected to agarose (0.8%) gel electrophoresis and the plasmid DNA was viewed in a gel documentation system.

2.3. Disinfection study

2.3.1. Colony forming units (CFU)

Samples collected at specific time intervals during disinfection experiments were serially diluted in physiological saline. 100 μL of serially diluted sample was inoculated in nutrient agar (Himedia, India) plates and incubated overnight at 37 °C. Colonies formed were counted with a colony counter. CFU mL^{-1} was calculated according to Eq. (2)

$$\mathrm{CFU}/\mathrm{mL} = \frac{\mathrm{No.\ of\ colonies} \times \mathrm{Dilution\ factor}}{\mathrm{Volume\ inoculated}} \quad (2)$$

2.3.2. ATP measurement

ATP is a measure of cell viability (Long et al., 2015). Total and free ATP for samples collected at specific time intervals were measured using Hygiena AquaSnap™ ATP Water Test swabs in an EnSUR Eluminometer (Sanna et al., 2018). The values obtained are in terms of Relative Light Units (RLU). ATP analysis was performed as per the manufacturer's instruction.

2.3.3. Dry cell weight

The effect of disinfection on cell mass reduction was studied. Samples collected before and after treatment at specific time intervals were centrifuged (5000 rpm) for 5 min. The pellet obtained was washed thrice with sterile distilled water and lyophilized (Bellali et al., 2020). The lyophilized samples were weighed to determine the dry cell weight as a function of time.

2.3.4. Fourier-transform infrared spectroscopy analysis

The effect of electrochemical disinfection on bacteria functional groups was studied with FTIR (Faghihzadeh et al., 2016). Samples collected before and after disinfection was centrifuged (5000 rpm) for 5 min. The cell pellet obtained was washed thrice with sterile distilled water and lyophilized. The lyophilized cell pellets were analyzed for functional group changes in FTIR (PerkinElmer, USA).

2.4. Quantification of ROS

•OH radicals generated at anode for different applied current density were quantified with Dimethyl sulfoxide (DMSO) as the trapping agent (Tai et al., 2004). The •OH radicals react with DMSO to form formaldehyde. The formaldehyde formed reacts with 2,4-Dinitrophenyl hydrazine (DNPH) to form DNPH-HCHO derivative. The resulting DNPH-HCHO derivative has an absorbance at 355 nm. Derivatized samples were analyzed in HPLC (Dionex Ultimate 3000, USA) with mobile phase acetonitrile: water (60:40) and flow rate 1 mL min^{-1} in a C_{18} column. Peaks corresponding to DNPH and DNPH-HCHO were observed at retention time 4.76 min and 7.32 min, respectively. However, it should be noted that the •OH radicals have a short life time and their interaction with DMSO is often incomplete. Hence, the determined •OH concentration is not absolute and only relative.

In order to understand the role of $SO_4^{\bullet-}$ in disinfection, 0.03 M tertiary-Butyl alcohol (*t*-BuOH) and 0.03 M Ethanol (EtOH) were separately added to 25 mM Na_2SO_4 with re-suspended cell pellets and disinfection experiments were performed at 30 mA cm^{-2} as mentioned in *section 2.2*. *t*-BuOH acts as a quencher for •OH (1.6–7.7 × 10^8 M^{-1} s^{-1}) and EtOH acts as a quencher for $SO_4^{\bullet-}$ (3.8–7.6 × 10^8 M^{-1} s^{-1}) (L. Chen et al., 2018). Samples were processed as mentioned in *section 2.3.1*.

2.5. Protein assay

Proteins released during disinfection were estimated by Bradford's assay with bovine serum albumin (Himedia, India) as standard (Bradford, 1976). Samples were withdrawn at specific time intervals and centrifuged at 5000 rpm for 5 min. Proteins in cell free supernatant and cell pellet after disruption were quantified. The sample was mixed with an appropriate volume of Bradford's reagent. The mixture was allowed to stand for 2 min at room temperature, and the absorbance was measured at 595 nm in a UV-spectrophotometer (Schimadzu, Japan).

2.6. DNA analysis

DNA released due to cell disruption and cytoplasm leakage during disinfection was confirmed by wavelength scan between 230 nm and 350 nm. Cell-free supernatant samples before and after disinfection withdrawn at specific time interval was subjected to wavelength scan. DNA from the cell pellet was isolated using DNA mini prep kit (Qiagen, India). Agarose (0.8%) (Himedia, India) gel electrophoresis was performed for both cell-free supernatant containing DNA and DNA isolated from cell pellets before and after treatment. The agarose gel was visualized in a gel documentation system (Gelstan, India).

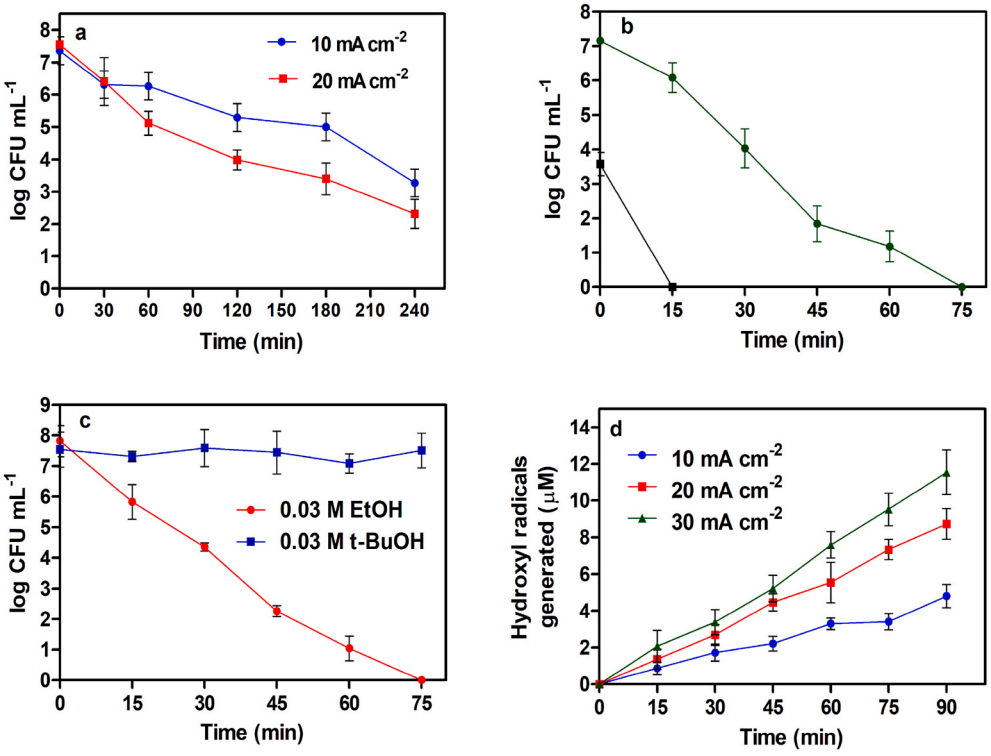

Fig. 2. Disinfection of *E. coli* using Ti/Sb–SnO_2/PbO_2 anode (a) Log reduction of *E. coli* at applied current densities 10 and 20 mA cm^{-2} (b) Log reduction of *E. coli* (different initial cell concentration) at applied current density 30 mA cm^{-2} (c) Disinfection of *E. coli* in 25 mM Na_2SO_4 electrolyte in the presence of 0.03 M ethanol or 0.03 M tertiary-butyl alcohol (d) Hydroxyl radicals generated at anode at applied current densities 10, 20, and 30 mA cm^{-2}. Data are mean values with standard deviation, n = 3.

2.7. SEM analysis

Morphology changes in *E. coli* cells during disinfection were visualized under SEM. Samples before and after treatment were withdrawn and centrifuged at 5000 rpm for 5 min. Cell pellet obtained was washed thrice with sterile distilled water and re-suspended in physiological saline. 50 μL of this was smeared on a coverslip and allowed to air dry. To facilitate conduction, samples were sputter-coated with gold and then observed under SEM (Quanta FEG 200, USA).

2.8. Zeta potential and cell size measurement

Change in cell potential, poly-dispersive index (PDI), and cell size due to the addition of Na_2SO_4 and during disinfection were studied. Samples at specific time interval were withdrawn to measure zeta potential, and electrophoretic mobility in a Zeta analyzer (Horiba Scientific Nanopartica, SZ 100) and values were estimated using Smoluchowski equation (Delgado et al., 2007).

2.9. Energy requirements and cost analysis

Energy required for disinfection of *E. coli* by EOP was estimated according to Eq. (3)

$$\text{Energy required, } E_{req} = \frac{U_{cell} I t}{V\ [(\Delta \log \frac{N_t}{N_0}]} \quad (3)$$

where, 'E_{req}' is the energy consumed per unit volume of water disinfected per log *E. coli* reduction (kWh/m^3), 'U_{cell}' is the average cell voltage (V), 'I' is the input current (A), 't' represents total disinfection time (h), 'V' is the volume of water subjected to disinfection (L), $\Delta \log \frac{N_t}{N_0}$ is the log reduction of *E. coli* at time 't'.

Cost analysis includes cost of electrode preparation, chemicals added to improve the conductivity and energy cost. Cost analysis becomes important to evaluate the feasibility for large adaptation of electro-oxidation for disinfection. The operational cost was estimated according to Eqs. (4)–(6)

$$\text{Energy consumed (Wh/L)} = \frac{U_{cell} I t}{[(\Delta \log \frac{N_t}{N_0}]\ \text{X Volume (L)}} \quad (4)$$

$$\text{Energy cost (₹/log } E.\ coli \text{ removed)} = \frac{\text{Energy consumed (Wh/L) X Electricity cost } (\frac{₹}{\text{kWh}})}{\left[(\Delta \log \frac{N_t}{N_0}\right] \text{X Volume (L)}} \quad (5)$$

$$\text{Chemical cost (₹/log } E.\ coli \text{ removed)} = \frac{\text{Chemical required } (\frac{\text{kg}}{\text{L}}) \text{ X unit cost of chemical } (\frac{₹}{\text{kg}})}{\left[(\Delta \log \frac{N_t}{N_0}\right] \text{X Volume (L)}} \quad (6)$$

3. Results and discussion

3.1. EOP disinfection using Ti/Sb–SnO_2/PbO_2 anode

3.1.1. Effect of applied current density

Disinfection of *E. coli* with initial concentration 10^7 CFU mL^{-1} was carried out at applied current density 10, 20, and 30 mA cm^{-2}, respectively. Fig. 2a and b shows log reduction of *E. coli* at different applied current density as a function of time. At an applied current density of 30 mA cm^{-2}, complete disinfection (7 log reduction) was observed at 75 min (disinfection rate constant, k_{obs} = 0.1048 min^{-1}). However, for applied current densities 10 and 20 mA cm^{-2}, at 75 min inactivation was 15.09% (k_{obs} = 0.0166 min^{-1}) and 32.85% (k_{obs} = 0.0422 min^{-1}), respectively. It is evident that disinfection occurs at a faster rate at high applied current density, as reported previously during *E. coli* disinfection with BDD electrode (Li et al., 2010). EOP disinfection is both current and viable *E. coli* concentration driven. In case of low applied current densities 10 and 20 mA cm^{-2} (Fig. 2a), the rate of disinfection is limited by applied current density, which leads to reduction in inactivation efficiency and increase in treatment time (Martínez-Huitle et al., 2015). Incase of applied current density 30 mA cm^{-2}, initially inactivation was current driven, which resulted in exponential bacteria death up to 45 min (Fig. 2b). After 45 min, a lag in disinfection was observed, which could be due to kinetics change brought about by decrease in number of viable cells. Initially, the numbers of viable cells were more and no mass transfer limitations with respect to live cells. Hence, at high current density exponential cell death was observed. After 45 min, it could be hypothesized that the decrease in viable cell number resulted in mass transfer limitations due to shielding of live cells by high number of dead cells in the bulk medium.

3.1.1.1. Predominant ROS in EOP disinfection. Disinfection of *E. coli* in a chlorine-free media is solely due to •OH radicals generated at the Ti/Sb–SnO_2/PbO_2 anode (Jeong et al., 2006; Li et al., 2010). Hence, •OH radicals were also quantified for different applied current densities (Fig. 2c). H_2O_2 generated at the cathode could also participate in disinfection. Jin et al. (2019) reported effective disinfection of *E. coli* by H_2O_2 using modified RVC cathode. However, stainless is used as cathode in the current study. Jin et al. (2019) also observed no generation of H_2O_2 on stainless cathode at neutral pH in Na_2SO_4 system. Moreover, studies that demonstrated production of H_2O_2 in an electrochemical system using stainless steel were surface modified and experiments were performed under acidic conditions (pH < 5.8) (Patra and Munichandraiah, 2009). Hence, it could be assumed that the participation of H_2O_2 in *E. coli* disinfection is negligible when stainless electrode is used as cathode and operated under neutral and near neutral pH (8.03 ± 0.39) such as the current study. Moreover, two-electron oxidation of water to produce H_2O_2 is less favored (E = 1.76 V/SHE) without a catalyst than the four-electron oxidation of water to produce O_2 (E = 1.23 V/SHE) (Sirés et al., 2014).

Similarly, $SO_4^{\bullet-}$ could also be generated during EOP in sulfate medium, which could enhance the disinfection process (Bruguera-Casamada et al., 2016). Disinfection rate was not significantly affected when EtOH was used to quench $SO_4^{\bullet-}$ (Fig. 2c). However, *in-situ* generation of $SO_4^{\bullet-}$ from sulfate ions during EOP cannot be ruled out. Studies reported effective generation of $SO_4^{\bullet-}$ in alkaline conditions (pH > 9) in sulfate medium (L. Chen et al., 2018). In the current study, pH of the system was recorded as 8.03 ± 0.39. Apart from pH, concentration

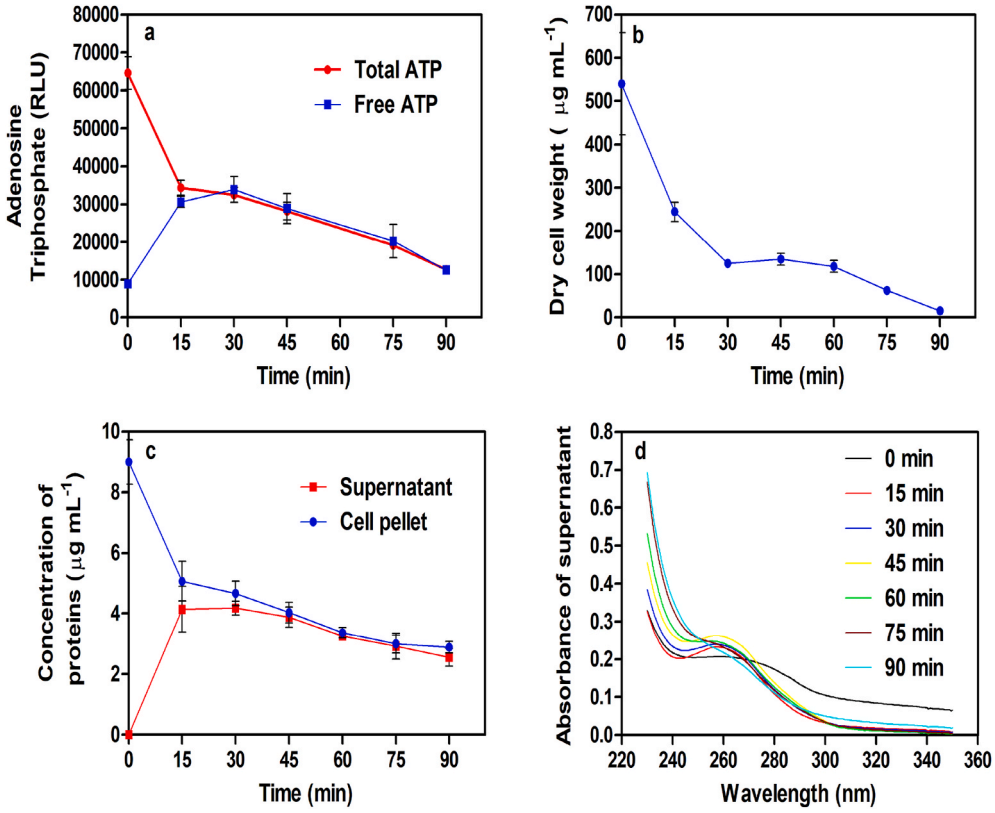

Fig. 3. (a) Change in ATP as a function of time at applied current density 30 mA cm^{-2} (b) Change in dry cell weight as a function of time at applied current density 30 mA cm^{-2} (c) Protein release and degradation at applied current density 30 mA cm^{-2} (d) Genetic material release during disinfection at applied current density 30 mA cm^{-2}. Data are mean values with standard deviation, n = 3.

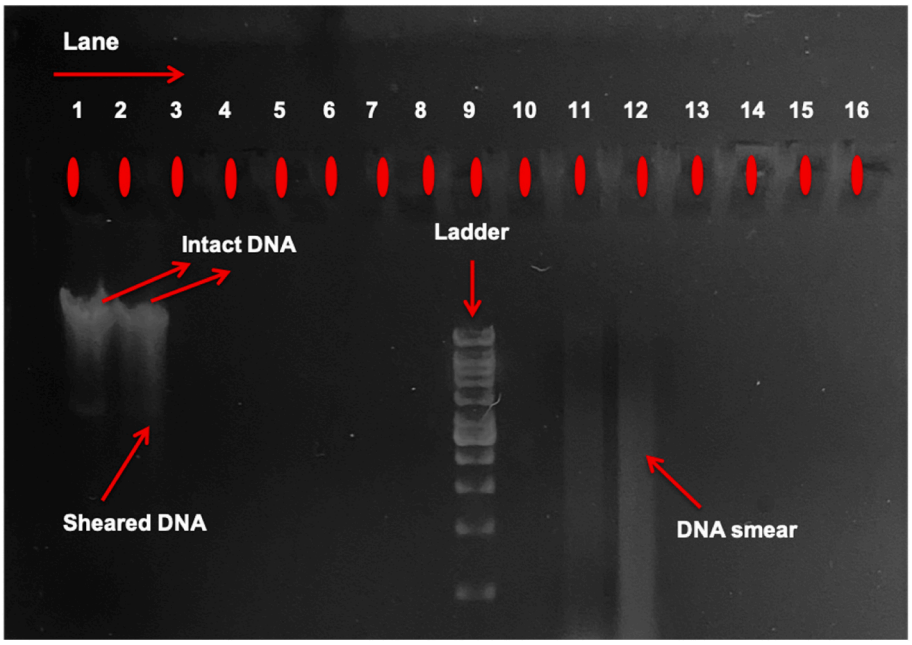

Fig. 4. DNA degradation during disinfection at applied current density 30 mA cm^{-2} (a) DNA isolated from the cells at specific time intervals (b) DNA isolated from cell-free supernatant at specific time intervals.

of sulfate ions also affect $SO_4^{\bullet-}$ generation. Effective generation of $SO_4^{\bullet-}$ in sulfate medium was observed with concentration of Na_2SO_4 above 100 mM (L. Chen et al., 2018). In the current study however, the experiments were carried out with 25 mM Na_2SO_4. This confirms that $SO_4^{\bullet-}$ has no significant role in disinfection of *E. coli* in the current study.

To further confirm the role of •OH, *t*-BuOH was used as quencher. As shown in Fig. 2c it could be seen that the *E. coli* inactivation was completely impaired due to unavailability of •OH. This observation confirmed that the predominant oxidant in EOP disinfection is •OH. Fig. 2d shows an increase in •OH radical concentration as a function of time for different applied current densities. A direct correlation was observed between increase in log reduction of *E. coli* and increase in •OH radical concentration with time. Initial lag in *E. coli* reduction was observed in the beginning of the experiment. This lag could be due to less •OH radicals generated initially resulting in low concentration of physisorbed •OH at the anode surface. Increasing the applied current density could also increase •OH radical concentration in the bulk media in the vicinity of the anode. However, at high-applied current densities parasitic reactions such as evolution of O_2 and H_2 at anode and cathode, respectively reduces current and process efficiency (Sirés et al., 2014). Apart from applied current density and viable cell number, hydrodynamics also plays an important role in determining the efficiency of disinfection. In batch EOP, mass transfer limitations contributed by *E. coli* cells could be improved by proper mixing. Uniform and effective mixing of the bulk medium reduces concentration gradient and ensures homogeneity thus enabling effective interaction between •OH and *E. coli* (Martínez-Huitle et al., 2015).

3.1.2. Effect of initial cell concentration

Disinfection of *E. coli* at initial concentrations of ~10^3 CFU mL^{-1} and ~10^7 CFU mL^{-1} was studied for the applied current density 30 mA cm^{-2}. Fig. 2b shows *E. coli* log reduction at different initial concentrations. For initial *E. coli* concentration 10^3 CFU mL^{-1} and 10^7 CFU mL^{-1}, complete disinfection was observed at 15 min and 75 min, respectively. Lower the initial cell concentration faster is the disinfection at high-applied current density. Jin et al. (2019) also reported reduction in disinfection time for low initial cell concentration using reticulated vitreous carbon (RVC) anode. This could be due to the high concentration of •OH radicals generated at a high-applied current density. Effect of initial cell concentration on EOP could be extrapolated from conditions and theories proposed for organic pollutants. Initial *E. coli* cell concentration determines the current and disinfection efficiency of EOP. In general, high initial cell concentration offers low mass transfer resistance and high current efficiency whereas, vice versa for low initial cell concentration (Martínez-Huitle et al., 2015). For low initial cell concentration, operating at optimum applied current density and effective mixing should essentially reduce the mass transfer resistance and increase the disinfection and current efficiency of the process.

3.1.3. Change in intracellular ATP

Log reduction in *E. coli* due to disinfection could be directly correlated with the free and total ATP measured in the system (Fig. 3a). ATP is a measure of active cells in a system (Osimani et al., 2014). Total ATP is the sum of intracellular ATP and free/dissolved ATP in a system (Pistelok et al., 2016). An increase in the trend of free ATP was observed at the beginning of the disinfection process. The release of intracellular ATP is due to cell death and degradation (Imamura et al., 2020). The increase in free ATP concentration is due to release of intracellular ATP (Mempin et al., 2013). At 30 min, total ATP was almost equal to free ATP, indicating absence of intracellular ATP due to rapid cell death during disinfection process. ATP generation could be affected by ROS interaction (Jin et al., 2016). Long et al. (2015) also reported a decrease in intracellular ATP during *E. coli* inactivation using BBD electrode. Moreover, evidence also suggest that interaction of •OH radicals with cell wall proteins alter the cell potential resulting in inhibition of cell multiplication and ATP synthesis (Bruguera-Casamada et al., 2016). Further reduction in ATP with time could be due to ATP degradation during the process. The concentration of ATP in a system is reported to decrease when bacteria in the system are dying (Mempin et al., 2013). ATP released by dead cells usually undergoes hydrolysis, which could result in ATP degradation (Bajerski et al., 2018). During disinfection, the ATP could also undergo electrolysis due to non-specific interaction of ROS, which resulted in extracellular ATP decrease with time.

3.1.4. Change in dry cell weight

Change in initial dry cell weight was observed as a function of time (Fig. 3b). Dry cell weight at 0 min was 539.82 ± 117.65 μg mL^{-1}. About 97.2% of the initial cell weight was oxidized at the end of 90 min

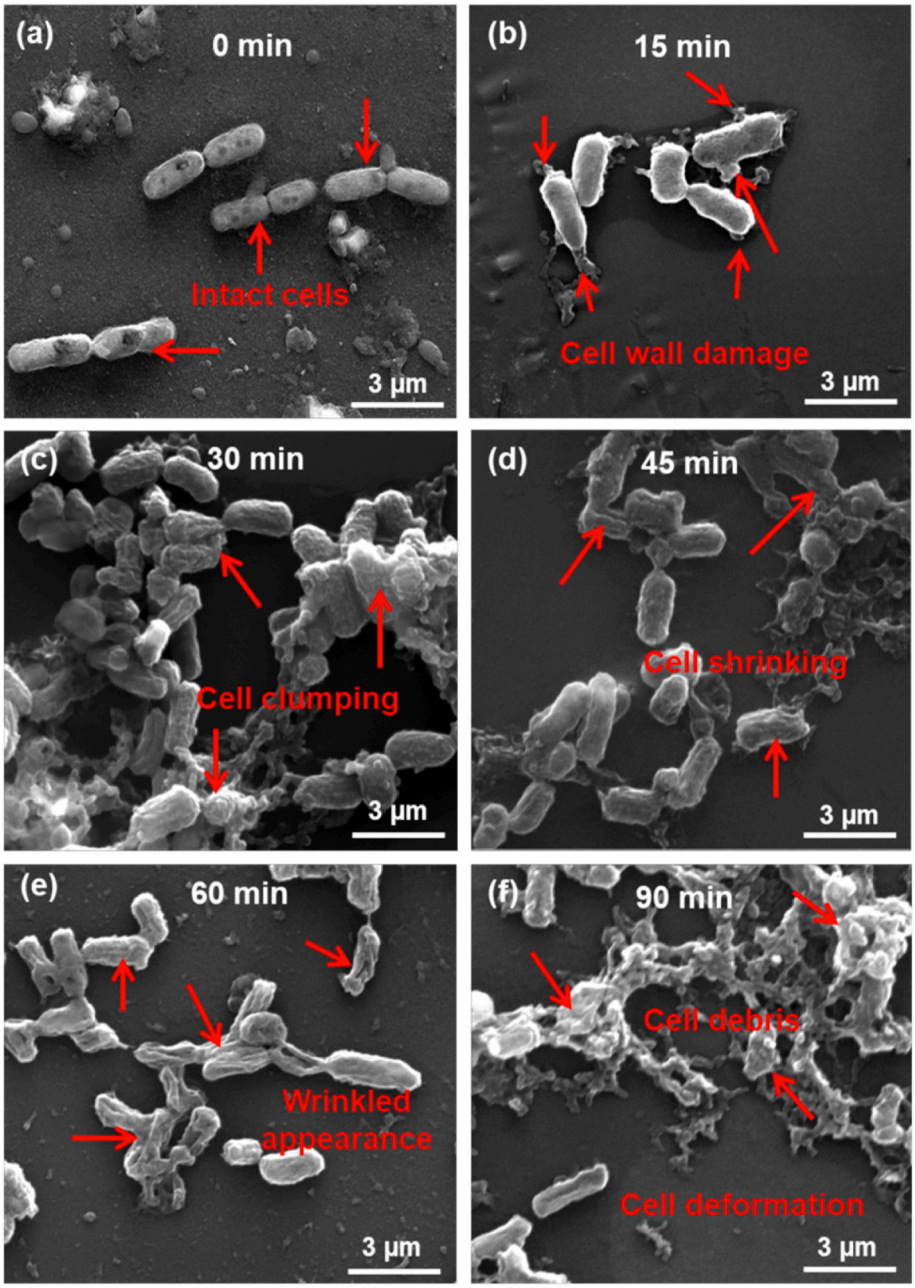

Fig. 5. Morphology changes in *E. coli* during disinfection at applied current density 30 mA cm^{-2} (a) Intact *E. coli* cells (before disinfection) (b–f) Morphology changes in *E. coli* at different time intervals during disinfection.

treatment. •OH radical is known to oxidize organic carbon, nitrogen and other organics such as carbohydrates, mono-, di-saccharides (Barragan et al., 2018; Holade et al., 2018). Reduction in protein concentration (Fig. 3c) and genetic material degradation (Figs. 3d and 4) were also observed, which is in correlation with the decrease in dry cell weight with treatment time. Reduction in cell mass could be due to release of intracellular organelles due to cell rupture and rapid oxidation of proteins, polysaccharides, genetic material, and other organic contents in *E. coli* cell (Singh et al., 2016).

3.2. Protein release and degradation

To understand protein release and degradation during disinfection, protein concentration in cell free supernatant and cell pellets after sonication were estimated. Initially, proteins were absent in the supernatant, indicating presence of intact cell wall and no cell lysis (Fig. 3c). At 15 min, protein concentration in the supernatant was found to increase while the concentration of intracellular protein isolated from the cell pellet decreased. This confirms that the increase in protein concentration in cell free supernatant is due to oxidative damage caused by •OH radicals, which resulted in cell wall damage, rupture, and protein release (Ghernaout et al., 2011; Zeng et al., 2019).

Increase in protein concentration trend was observed in the supernatant until 45 min (Fig. 3c). At 60 min, concentration of protein in the cell free supernatant (3.26 ± 0.13 μg mL^{-1}) and protein in cell pellets (3.38 ± 0.17 μg mL^{-1}) were almost equal. From there on, decrease in protein concentration for both cell free supernatant and cell pellet was observed. Singh et al. (2016) also observed decrease in both intracellular and extracellular protein concentration upon plasma disinfection of *E. coli*. This could be due to peptide cleavage and protein damage caused by •OH during electrochemical disinfection (Jin et al., 2016). Amino acid residues such as cysteine and methionine easily undergo electro

oxidation (Pei et al., 2015). Oxidation of specific amino acid residues would result in peptide cleavage. Further interaction between ROS and peptides during electrolysis could degrade and oxidize peptides followed by oxidation of amino acids that results in reduction of extracellular protein concentration (Pei et al., 2018). Long et al. (2015) also observed membrane protein damage, leakage, oxidative protein damage and degradation in *E. coli* during electrochemical inactivation using BDD electrode, which is consistent with the current study.

3.3. Genetic material release, fragmentation, and degradation

To understand the genetic material release during the treatment, UV spectrum scan was performed for cell-free supernatant. Fig. 3d represents the DNA spectrum of cell-free supernatant sampled at specific time intervals during disinfection. At 0 min, the corresponding curve was almost flat, indicating no genetic material in the cell-free supernatant. An increase in the peak height at 260 nm was observed until 45 min. This could be due to rapid DNA release during cell lysis and death in the early stage of treatment (Pillet et al., 2016). Cell wall damages caused due to oxidation of phospholipids and proteins of cell membrane by •OH affects the cell integrity. Further, oxidative cell wall damage leads to cell rupture and release of cell organelles such as DNA. Hence, an increase in supernatant DNA concentration was observed with time (Sharma et al., 2012). A gradual decrease in the peak height after 45 min was observed, which could be due to the degradation of genetic material with increased treatment time. •OH radicals interact with nucleic acids and cause DNA strand breakage (Ghernaout et al., 2011). Nucleic acid release, concentration increase in cell-free supernatant, and fragmentation could happen during the inactivation of *E. coli* due to ROS interaction (Pillet et al., 2016; Singh et al., 2016). Apart from oxidative strand breakage, •OH is also known to cause modification and removal of nucleotide bases, which leads to DNA damage and fragmentation (Sharma et al., 2012). Hence, a decrease in extracellular DNA concentration was observed.

Fig. 4 represents the DNA isolated before and after disinfection from cell pellets and cell-free supernatant, respectively. Lane 1 in Fig. 4 represents the DNA isolated from cell pellets at 0 min. The band was intact, which indicates that the cells were alive with an intact cell membrane at the beginning of the treatment. Lane 2 corresponds to DNA isolated from samples collected at 15 min of disinfection. It can be seen that the intensity of the DNA band decreased and DNA was smeared. Smear is due to DNA fragmentation during the disinfection process. However, no band was observed in the consecutive lanes. This could be due to fragmentation and degradation of DNA, resulting in concentration reduction below visualization limits. Lane 10 in Fig. 4 represents the DNA isolated from cell-free supernatant at 0 min where no DNA band was observed. Further, control experiments were conducted to eliminate false-positive results, which confirmed that cells adapted to the electrolyte and majority of cell death or lysis occurred only due to the interaction of •OH radical generated at the anode (Fig. S2). DNA smear was observed in lane 11 and lane 12, which corresponds to extracellular DNA isolated from the cell free supernatant of samples collected at 15 min and 30 min, respectively. Shearing of DNA results in smear, which is due to interaction of •OH with DNA resulting in fragmentation (He et al., 2019). However, an increasing trend in DNA release was observed up to 45 min (Fig. 3d). This is because DNA fragmentation does not affect the absorbance at 260 nm and hence an increase in trend was observed. DNA analysis confirms that oxidative damage results in cell lysis, genetic material release and fragmentation/degradation.

DNA leakage, damage, fragmentation, and degradation were also previously reported during disinfection of *E. coli* with plasma (Singh et al., 2016), photo irradiation (Hirakawa et al., 2004), electrochemical oxidation (Reipa et al., 2018) and photo-electrocatalytic process (H. Sun et al., 2014). However, no attempt was made to understand the mechanism clearly. To further confirm the fragmentation, and degradation of extracellular/genetic material released, plasmid degradation study was carried out. Plasmid DNA exists in nicked, linear, supercoiled, or circular confirmations. Fig. S3 shows the plasmid DNA isolated from samples before and after electrochemical treatment. Lane 2 represents plasmid DNA isolated from sample at 0 min. However, at 15 min (Lane 3), no visible band was observed. This is due to rapid fragmentation and degradation of plasmid DNA during treatment. This confirms that DNA released due to cell lysis and death also undergoes rapid oxidation.

Table 1
Change in zeta potential, cell size, electrophoretic mobility and poly-dispersive index of *E. coli* during disinfection at applied current density 30 mA cm^{-2}

Time (min)	Z - average (μm)	Zeta-potential (mV)	Electrophoretic mobility ($cm^2V^{-1}s^{-1}$) (10^{-6})	Poly-dispersive index
0	2.71 ± 0.8	−13.9 ± 3.8	−108 ± 27	0.416 ± 0.11
15	4.89 ± 0.1	−3.7 ± 0.9	−29 ± 8	2.6 ± 0.5
30	>10	−0.2 ± 0.1	−18 ± 6	–
45	>10	−0.8 ± 0.2	−6 ± 2	–
60	>10	−0.6 ± 0.3	−5 ± 1	–
75	4.8 ± 0.4	−11.9 ± 2.6	−92 ± 18	1.58 ± 0.2
90	2.3 ± 0.2	−17.4 ± 3.1	−135 ± 5	2.263 ± 0.6

3.4. Changes in E. coli morphology

In order to understand physical alterations in the *E. coli* cell membrane and deformities SEM analysis was for samples collected at different time intervals of the disinfection process at an applied current density 30 mA cm^{-2}. Fig. 5a-f confirms the changes in cell structure and surface morphology of *E. coli* cells.

Fig. 5a shows intact rod cells with smooth surface and the average size of 2 μm before the disinfection process. Initially, cell wall damage (Fig. 5b) was observed at 15 min with cytoplasm exuding out of the cells. The severity of cell membrane damage increased with time due to increased exposure to a high concentration of •OH radicals generated at a high-applied current density. Irregularities in the cell membrane is due to micropores that are formed due to •OH radicals' interaction with the cell membrane (Osimani et al., 2014). Interaction of ROS with cell membrane protein could result in alteration of protein structure resulting in irregularities in the cell membrane (Libardo et al., 2017). The cell wall damage however, is not uniform due to the non-specific interaction of •OH radicals, which is further confirmed by the FTIR spectrum, where no specific change in appearance or disappearance of the peaks corresponding to functional groups were observed (Fig. S5). Cell wall damage was followed by cell clumping (Fig. 5c) and cell shrinking (Fig. 5d). Cell clumping could be due to a slight increase in pH during disinfection leading to decrease in cell surface potential that favors agglomeration of cells(Fig.S4). On the other hand, and cell shrinking could be due to leakage of cell components. Clumped cells further shrank to give a wrinkled appearance (Fig. 5e) due to extensive cell damage and leakage of cell components (G. Sun et al., 2021; X. Zhang et al., 2019b). Extending disinfection time up to 90 min resulted in extensive oxidative cell damage (Fig. 5f). Cell debris due to rupture and cell wall damage was observed, indicating that cells are no longer viable, and the damage is irreversible. No regrowth was observed, which further confirms the irreversible cell death (S5). Destabilization and clumping of *E. coli* cells with applied current density are in accordance with the measured zeta potential and cell size (Table 1).

3.5. Change in zeta potential and cell size

Zeta potential analysis and cell size measurements were performed to understand the effect of •OH generated and changes in membrane potential during disinfection due to applied current density (Table 1). Zeta potential of *E. coli* cells before suspension in 25 mM Na_2SO_4 electrolyte was −79.2 mV, and the size was ~2 μm, which is the characteristic cell size of *E. coli*. The net negative charge of *E. coli* is due to the

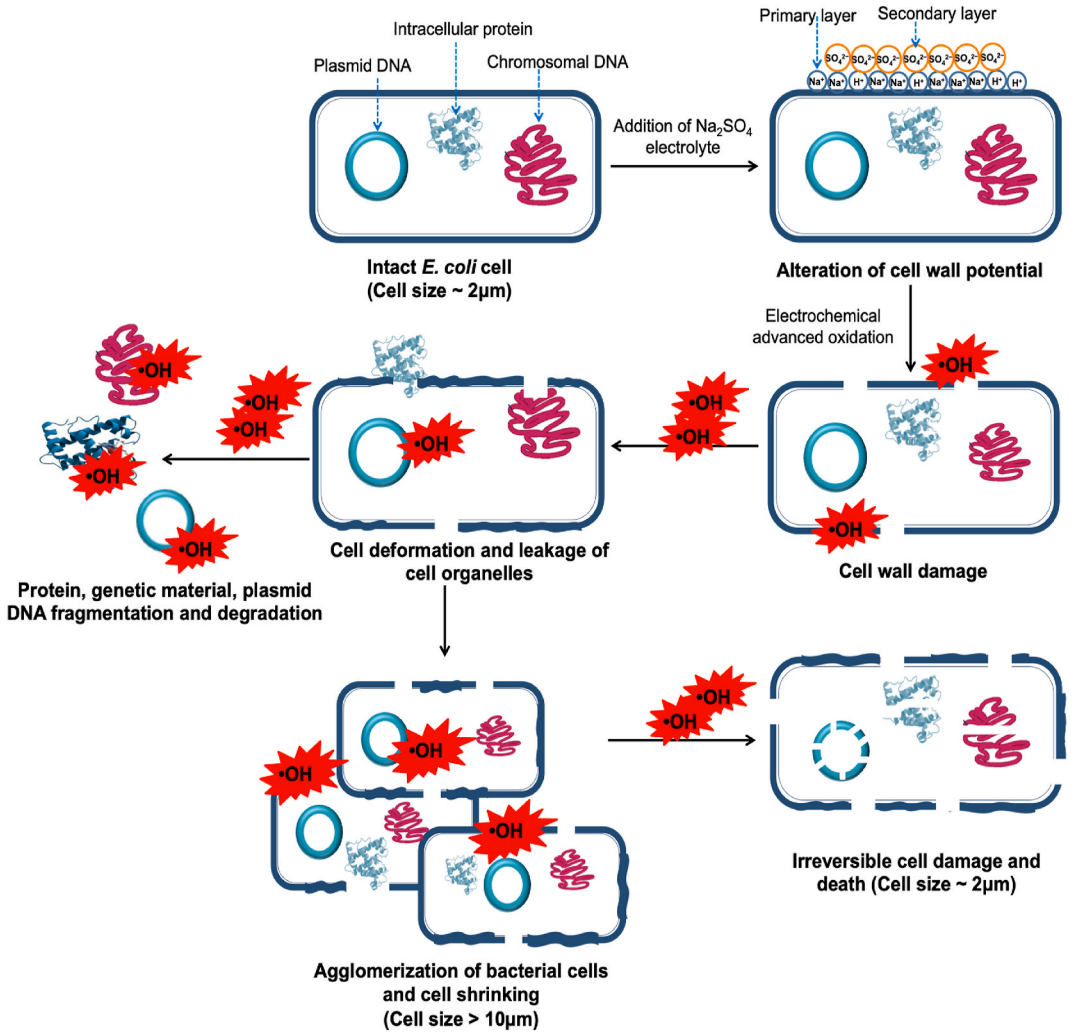

Fig. 6. Proposed *E. coli* inactivation mechanism during electro-oxidation process.

presence of membrane functional groups such as lipopolysaccharide, proteins, lipoproteins, and extracellular polymeric substance that stabilizes bacterial cells in an aqueous suspension (Alves et al., 2010; Taylor et al., 2014). A decrease in zeta potential to −13.9 mV was observed for cells suspended in 25 mM Na_2SO_4 electrolyte upon treatment. Membrane potential of *E. coli* changes due to electrolyte addition (Taylor et al., 2014). This is mainly due to the double layer that is formed around *E. coli* cells during disinfection. *E. coli* cells attract positive ions in solution to achieve electroneutrality (Diaz et al., 2021). Positively charged Na^+ ions forms a primary layer around *E. coli* cells, thus neutralizing the negative charge of *E. coli* and altering cell membrane potential. The second layer of SO_4^{2-} surrounds the primary layer. The double-layer formed stabilizes bacteria in a solution. Hence, the bacterial membrane potential was observed to change from −79.2 mV to −13.9 mV. Reduction in zeta potential could also be due to reduction in cell viability and metabolic activity (Lee et al., 2018; Singh et al., 2016).

Change in membrane potential affects the stability and integrity of the cell membrane that alters the membrane permeability resulting in leakage of intracellular components (Halder et al., 2015). During disinfection, the release of intracellular components could result in overage of the bacterial cell membrane and neutralizes the membrane functional groups. This causes the destabilization of bacterial colloids. Zeta potential approached less negative from −13.9 mV at 30 min due to destabilization. Destabilization causes cell agglomeration. In addition, cell size was observed to increase from ~2 μm to ~10 μm during disinfection up to 60 min due to cell clumping. Agglomeration of *E. coli* under applied current density could be a mechanism of shielding from ROS during disinfection (Lee et al., 2018).

Agglomeration or cell clumping is evident from SEM image analysis (Fig. 5c–e). Severe damage and deformities caused by •OH radical alter the cell membrane potential. As a result of charge neutralization and increase in cell size, electrophoretic mobility of the cells was observed to decrease (become less negative) from $-108*10^{-6}$ to $-5*10^{-6}$ $cm^2 V^{-1}s^{-1}$. As the cell membrane charge is neutralized, bacteria cells aggregate together losing electrophoretic mobility in the solution, which is in accordance with the zeta potential values (Table 1). Electrophoretic mobility of neutral particles is virtually zero (Stalcup, 2006). At 90 min, a decrease in cell size, negative increase in zeta potential and electrophoretic mobility was observed. The zeta potential of dead *E. coli* cells were observed to be around −20 mV (Kłodzińska et al., 2010). This could be due to cell debris resulting from oxidation of cell membrane and cell components by highly active radical species. SEM analysis at 90 min confirms irreversible damage and cell death (Fig. 5f). Change in the poly-dispersive index was observed due to heterogeneity in bacterial cell size as a result of zeta potential change and agglomeration of cells during electro-oxidation (Singh et al., 2016) (Table 1).

3.6. Proposed E. coli inactivation mechanism

Several EOP disinfection studies have been reported (Bruguera-Casamada et al., 2016; Lacasa et al., 2013; Li et al., 2010; Long et al., 2015; Thostenson et al., 2018). However, inactivation mechanism is not

Table 2
Wastewater characteristics before and after disinfection.

Parameter	Initial	Final	Removal (%)
COD (mg L^{-1})	88 ± 11.3	20.8 ± 6.78	76.36
Bacterial count (log CFU mL^{-1})	3.47 ± 0.03	0	~99.99
ATP (RLU)	392 ± 9.89	0	100
Chlorides (mg L^{-1})	304.91 ± 1.41	213.86 ± 3.92	29.86
Phosphate (mg L^{-1})	3.8 ± 1.2	3.4 ± 0.6	10.52
Ammonia Nitrogen (mg L^{-1})	7.86 ± 1.72	5.23 ± 1.8	33.46
pH	7.3 ± 0.04	8.25 ± 0.10	–
Conductivity (mS cm^{-1})	4.58 ± 0.028	4.655 ± 0.092	–

clearly understood. Fig. 6 represents the proposed *E. coli* inactivation mechanism in Ti/Sb–SnO_2/PbO_2 and Na_2SO_4 electrolyte system. The mechanism is described based on SEM images (Fig. 5 a-f), changes in dry cell weight (Fig. 3b), protein release and degradation (Fig. 3c), DNA release, fragmentation and degradation (Figs. 3d and 4, S4), zeta potential, and cell size measurement (Table 1).

The addition of electrolyte to cell (−79.2 mV) decreases negative charge (−13.9 mV) of the cell altering the cell membrane potential. However, cell size (~2 μm) remains the same. When cells in the electrolyte are subjected to disinfection, i) Cell wall is oxidatively damaged resulting in cell inactivation ii) Cell membrane potential negatively decreases (−3.7 mV) resulting in cell size increase (~4.89 μm) due to cell clumping. iii) Cell wall damage results in leakage of intracellular organelles. iv) Further electrolysis results in cell shrinking, a negative decrease of cell membrane potential (−0.2 mV), and cell clumping/agglomeration (>10 μm size). v) Since •OH radicals are not specific in interaction, released cell organelles such as proteins, genetic material, and plasmid DNA also undergo damage, oxidative fragmentation, and degradation. vi) Further disinfection causes cell deformation, de-agglomeration of cells resulting in cell size reduction (~4.8–2.3 μm). Since the cells are dispersed, cell membrane potential negatively increases (−17.4 mV). vii) Prolonged disinfection results in irreversible cell damage and death.

3.7. Disinfection of real wastewater

To evaluate the disinfection efficiency, experiments were conducted with secondary effluent collected from IIT Madras sewage treatment plant, Chennai, TN, India. Table 2 presents the wastewater characteristics before and after disinfection. 150 mL of *E. coli* cells suspended in the electrolyte was replaced with wastewater for this part of the study. The conductivity of effluent was 1.153 ± 0.005 μS cm^{-1}. Hence, 25 mM of Na_2SO_4 was added to provide sufficient conductivity for electrolytic disinfection. The disinfection experiment was conducted at an applied current density 30 mA cm^{-2}.

3.5 log reduction was achieved in 12 min, which is comparable with disinfection efficiency of synthetic wastewater containing 10^3 CFU mL^{-1} initial *E. coli* concentration (Fig. 2b). Zero ATP after disinfection indicates no live cell in the system. 76.36% of COD removal was achieved in 12 min. Total chloride in the wastewater was 304.91 ± 1.41 mg L^{-1}. Enhanced disinfection of wastewater despite high COD compared to synthetic wastewater could be due to the presence of co-oxidants generated due to oxidation of chloride and sulfate ions in wastewater. Presence of ions such as ammonia nitrogen and phosphates in high concentration could reduce the disinfection efficiency due to scavenging of ROS generated and utilization of ROS for undesired reactions such as solubilization of phosphates and oxidation of ammonia nitrogen (Rajasekhar et al., 2020). However, the observed concentration of ammonia nitrogen and phosphates in this study are low (Table 2). Moreover, the reactivity of •OH radical towards ammonia nitrogen and phosphates is rather slow (Deng and Ezyske, 2011; Gray et al., 2020). Hence, the presence and effect of ammonia nitrogen and phosphates on disinfection efficiency could be considered negligible. Further, structural changes in bacteria during disinfection were observed in wastewater samples. SEM images of the observed changes in bacteria confirmed cell damage, disruption and death (Fig. S6). Moreover, from synthetic and actual wastewater sample it could be confirmed that effective electrochemical disinfection of wastewater could be achieved in a short time using Ti/Sb–SnO_2/PbO_2 anode.

3.8. Energy requirements and cost analysis

Fig. 7a represents the energy required for disinfection of synthetic wastewater at applied current densities 10, 20 and 30 mA cm^{-2}. Energy consumed in 1.25 h for 7 log reduction *of E. coli* was 17.228 kWh m^{-3} for applied current density 30 mA cm^{-2}. Whereas, the energy consumed at applied current density 20 mA cm^{-2} was 6.3 kWh m^{-3}, which achieved only for 2 log reduction of *E. coli* in 1.25 h. Similarly, the energy consumed for applied current density 10 mA cm^{-2} was 3.8 kWh m^{-3}, which resulted in only 1.2 log reduction of *E. coli* in 1.25 h. Fig. 7b represents the energy consumed for disinfection of synthetic and secondary treated real wastewater at applied current density 30 mA cm^{-2}. It could be seen that 3 log reduction *of E. coli* present in synthetic wastewater consumed 6.511 kWh m^{-3} of energy in 0.25 h. Whereas, the energy consumed in 0.2 h for 3.5 log reduction of bacteria in secondary treated wastewater was 4.978 kWh m^{-3}.

At low applied current density the energy consumed was low for equivalent disinfection time. However, the disinfection efficiency was only 15.09% (10 mA cm^{-2}) and 32.85% (20 mA cm^{-2}) compared to ~99.9% removal at applied current density 30 mA cm^{-2}. Energy

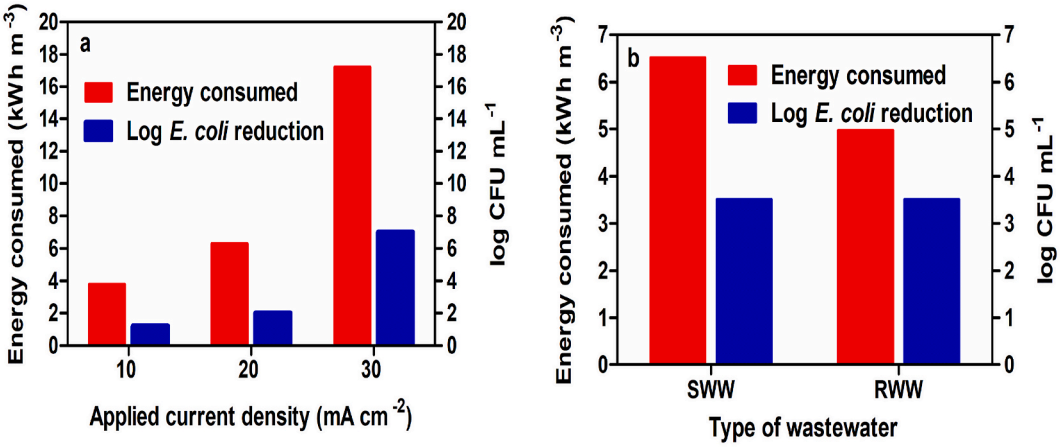

Fig. 7. (a) Energy required for disinfection of synthetic wastewater at applied current densities 10, 20 and 30 mA cm^{-2} (b) Energy required for disinfection of synthetic wastewater (SWW) and real wastewater (RWW) at applied current density 30 mA cm^{-2}.

Table 3
Concentration of Pb ions in the samples of control experiment-2 collected after 7 days of electrolysis.

Applied current density (mA cm^{-2})	Pb concentration (μg L^{-1})
10	0.32 ± 0.01
20	0.07 ± 0.006
30	0.002 ± 0.0003

consumed for real wastewater disinfection was ~1.3 times lower than the energy consumed for synthetic wastewater disinfection. This could be due to the presence of co-ions and co-oxidants in the real wastewater, which enhances the current and disinfection efficiency of the process (Jasper et al., 2017; Thostenson et al., 2018). The energy consumed per unit volume of water disinfected per log *E. coli* reduction by different electrochemical advanced oxidation processes (EAOP) as reported by (Kourdali et al., 2018) was ~13 kWh m^{-3}, ~5 kWh m^{-3}, and ~1 kWh m^{-3} for ~1.5, ~2.5 and ~7.5 log reduction of *E. coli* by electro-coagulation, reduction of *E. coli* by electro-peroxi-coagulation and electro-Fenton, respectively (Kourdali et al., 2018). Comparing the energy consumed by different EAOP disinfection techniques for 7.5 log reduction of *E. coli*, electro-fenton seems to be less energy consuming followed by EOP (current study), electro-peroxi-coagulation and electro-coagulation. The major disadvantages of electro-fenton process are addition of catalyst, recovery of catalyst and generation of iron sludge (M. Zhang et al., 2019a). EOP on the other hand, requires no addition of catalyst and no sludge is generated.

Total cost of operation is the sum of energy cost and chemical cost. The cost of operation for ~3.4 log reduction of *E. coli* in synthetic sample was 2900₹ and for ~3.5 log reduction of *E. coli* in real wastewater was 2800₹ for applied current density 30 mA cm^{-2}. Whereas, for 7 log reduction the cost of operation was 1400₹. The total cost of operation has a good correlation with initial *E. coli* concentration and chemical added at optimized operating conditions of volume and applied current density (Tripathy et al., 2020). Cost of disinfecting a real wastewater is relatively less compared to that of the synthetic wastewater, which can be correlated to the presence of co-ions. Presence of co-ions increases the energy efficiency of the process thus decreasing the cost of operation. If the wastewater has enough conductivity addition of chemical can be completely avoided and total cost of operation will be reduced by 1300₹ - 2800₹. For 8 MLD treatment plant, the total cost of EOP disinfection is about 1.3 million ₹ per annum assuming that the wastewater has enough conductivity.

3.9. Electrode stability and role of lead ions in disinfection

Two control experiments were performed to check i) whether the PbO_2 electrode is toxic to bacteria (Control experiment-1) and ii) whether the Pb^{2+} ions are released into the solution during electrolysis (Control experiment-2). In control experiment-1, experimental conditions viz; volume-150 mL, rpm- 150 ± 20, Na_2SO_4 – 25 mM, pH- 8.02 ± 0.27, and initial cell concentration- ~10^8 CFU mL^{-1} were maintained but the current was not applied across the electrodes. The samples collected for 180 min at regular intervals were plated on agar plates and CFU mL^{-1} was determined. No significant change was observed in the CFU mL^{-1} with time. The results of control experiments (Fig. S2) can be found in the supplementary information. The sample collected at 180 min was also subjected to ICP-OES analysis to the quantify Pb ions released into the solution. However, Pb ion concentration in the treated solution was below the detection limit. The results indicate that the Pb ions are not released into solution. Moreover, PbO_2 crystals are insoluble in water and it is less likely for Pb ions to directly contribute to electro-oxidation process. In other words, it is evident that bacteria even when it comes in contact with PbO_2 anode at the interface of the electrode-electrolyte are not killed, which implicates that PbO_2 is not toxic to the bacteria.

In control experiment-2, experimental conditions viz; volume-150 mL, rpm- 150 ± 20, Na_2SO_4 – 25 mM, pH- 8.02 ± 0.27 were maintained and current densities 10,20, 30 mA cm^{-2} were applied across the electrodes. The samples collected at the end of the 7 days were subjected to ICP-OES analysis and the results are provided in Table 3. The concentration of Pb ions were found to be decreasing with increasing applied current density. Decrease in PbO_2 ion concentration with increasing current density could also be due to the fact that PbO_2 was electrodeposited at 30 mA cm^{-2}. It is also reported that the stability of the PbO_2 anode prepared and operated at applied current density 30 mA cm^{-2} has more structural stability, since PbO_2 is anodically deposited and operated as anode (Velichenko et al., 2002). Samples collected from disinfection experiments conducted at applied current density 30 mA cm^{-2} with synthetic and real wastewater at 90 min and 15 min, respectively were also subjected to ICP-OES analysis. However, no Pb ions were detected in either of the samples. Only a small amount of Pb is detected in the samples of the control experiments, which is very much less than the Indian standard for drinking water (10 μg L^{-1})(IS-10500, 2012; WHO, 2017). The results suggest that PbO_2 electrodes are stable and suitable for effective disinfection real wastewater.

4. Conclusion

This study demonstrates enhanced and effective electrochemical disinfection with Ti/Sb–SnO_2/PbO_2 and Na_2SO_4 electrolyte system. An attempt was made to explore and understand the mechanism *E. coli* inactivation during EOP disinfection. •OH radical is highly reactive due to its high oxidation potential; hence high disinfection efficiency could be achieved when EOP is employed. The study confirms cell death, irreversible damage, and degradation of cell organelles proving effective disinfection. Effective disinfection eliminates the possibility of regrowth in distribution system, which is important when treated wastewater is reused or discharged into natural water bodies. Energy required is also comparatively low than the other EAOP processes. Moreover, EOP is simple; neither requires addition of catalyst nor generates sludge after treatment. High disinfection efficiency, and less/no requirement of chemical addition makes this treatment a better wastewater treatment option. Expensive BDD electrode could be replaced with the low cost Ti/Sb–SnO_2/PbO_2 electrode for water and wastewater treatment without compromising the disinfection efficiency. Future studies could be attempted i) to explore the application of other low-cost electrodes for disinfection, ii) to understand the effect of pH, electrolyte concentration, and other operating parameters, and iii) to reduce energy consumption.

Declaration of competing interest

The authors declare that they have no known competing financial interests or personal relationships that could have appeared to influence the work reported in this paper.

Acknowledgements

This work was supported by Indian Council of Medical Research, Government of India (F.No.AMR /146/2018-ECD-II). We would also like to acknowledge Ms. Velvizhi Devi R.'s assistance in DNA analysis.

Appendix A. Supplementary data

Supplementary data to this article can be found online at https://doi.org/10.1016/j.envres.2022.112749.

References

Abu Ghalwa, N., Hamada, M., Abu Shawish, H.M., Shubair, O., 2016. Electrochemical degradation of linuron in aqueous solution using Pb/PbO2 and C/PbO2 electrodes. Arab. J. Chem. 9, S821–S828. https://doi.org/10.1016/j.arabjc.2011.08.006.

Alves, C.S., Melo, M.N., Franquelim, H.G., Ferre, R., Planas, M., Feliu, L., Bardají, E., Kowalczyk, W., Andreu, D., Santos, N.C., Fernandes, M.X., Castanho, M.A.R.B., 2010. Escherichia coli cell surface perturbation and disruption induced by antimicrobial peptides BP100 and pepR. J. Biol. Chem. 285 (36), 27536–27544. https://doi.org/10.1074/jbc.M110.130955.

Bajerski, F., Stock, J., Hanf, B., Darienko, T., Heine-Dobbernack, E., Lorenz, M., Naujox, L., Keller, E.R.J., Schumacher, H.M., Friedl, T., Eberth, S., Mock, H.-P., Kniemeyer, O., Overmann, J., 2018. ATP content and cell viability as indicators for cryostress across the diversity of life. Front. Physiol. 9 https://doi.org/10.3389/fphys.2018.00921.

Bakheet, B., Islam, M.A., Beardall, J., Zhang, X., McCarthy, D., 2018. Electrochemical inactivation of Cylindrospermopsis raciborskii and removal of the cyanotoxin cylindrospermopsin. J. Hazard Mater. 344, 241–248. https://doi.org/10.1016/j.jhazmat.2017.10.024.

Barragan, J.T.C., Kogikoski, S., da Silva, E.T.S.G., Kubota, L.T., 2018. Insight into the electro-oxidation mechanism of glucose and other carbohydrates by CuO-based electrodes. Anal. Chem. 90 (5), 3357–3365. https://doi.org/10.1021/acs.analchem.7b04963.

Bellali, S., Bou Khalil, J., Fontanini, A., Raoult, D., Lagier, J.-C., 2020. A new protectant medium preserving bacterial viability after freeze drying. Microbiol. Res. 236, 126454. https://doi.org/10.1016/j.micres.2020.126454.

Bradford, M.M., 1976. A rapid and sensitive method for the quantitation of microgram quantities of protein utilizing the principle of protein-dye binding. Anal. Biochem. 72 (1), 248–254. https://doi.org/10.1016/0003-2697(76)90527-3.

Bruguera-Casamada, C., Sirés, I., Prieto, M.J., Brillas, E., Araujo, R.M., 2016. The ability of electrochemical oxidation with a BDD anode to inactivate Gram-negative and Gram-positive bacteria in low conductivity sulfate medium. Chemosphere 163, 516–524. https://doi.org/10.1016/j.chemosphere.2016.08.042.

Chen, L., Lei, C., Li, Z., Yang, B., Zhang, X., Lei, L., 2018. Electrochemical activation of sulfate by BDD anode in basic medium for efficient removal of organic pollutants. Chemosphere 210, 516–523. https://doi.org/10.1016/j.chemosphere.2018.07.043.

Chen, S., Hu, W., Hong, J., Sandoe, S., 2016. Electrochemical disinfection of simulated ballast water on PbO2/graphite felt electrode. Mar. Pollut. Bull. 105 (1), 319–323. https://doi.org/10.1016/j.marpolbul.2016.02.003.

Cuerda-Correa, E.M., Alexandre-Franco, M.F., Fernández-González, C., 2020. Advanced oxidation processes for the removal of antibiotics from water. An overview. Water 12 (1), 102. https://doi.org/10.3390/w12010102.

Dan, L., Zeng, S., Gu, A.Z., He, M., Shi, H., 2013. Inactivation, reactivation and regrowth of indigenous bacteria in reclaimed water after chlorine disinfection of a municipal wastewater treatment plant. J. Environ. Sci. 25 (7), 1319–1325. https://doi.org/10.1016/S1001-0742(12)60176-4.

Delgado, A.V., González-Caballero, F., Hunter, R.J., Koopal, L.K., Lyklema, J., 2007. Measurement and interpretation of electrokinetic phenomena. J. Colloid Interface Sci. 309 (2), 194–224. https://doi.org/10.1016/j.jcis.2006.12.075.

Deng, Y., Ezyske, C.M., 2011. Sulfate radical-advanced oxidation process (SR-AOP) for simultaneous removal of refractory organic contaminants and ammonia in landfill leachate. Water Res. 45 (18), 6189–6194. https://doi.org/10.1016/j.watres.2011.09.015.

Diaz, L., Li, Y., Jenkins, D.M., 2021. Chemical stabilization of dispersed Escherichia coli for enhanced recovery with a handheld electroflotation system and detection by Loop-mediated Isothermal AMPlification. PLoS One 16 (1), e0244956. https://doi.org/10.1371/journal.pone.0244956.

Elaissaoui, I., Akrout, H., Grassini, S., Fulginiti, D., Bousselmi, L., 2019. Effect of coating method on the structure and properties of a novel PbO2 anode for electrochemical oxidation of Amaranth dye. Chemosphere 217, 26–34. https://doi.org/10.1016/j.chemosphere.2018.10.161.

Faghihzadeh, F., Anaya, N.M., Schifman, L.A., Oyanedel-Craver, V., 2016. Fourier transform infrared spectroscopy to assess molecular-level changes in microorganisms exposed to nanoparticles. Nanotechnol. Environ. Eng. 1 (1), 1. https://doi.org/10.1007/s41204-016-0001-8.

Foster, H.A., Ditta, I.B., Varghese, S., Steele, A., 2011. Photocatalytic disinfection using titanium dioxide: spectrum and mechanism of antimicrobial activity. Appl. Microbiol. Biotechnol. 90 (6), 1847–1868. https://doi.org/10.1007/s00253-011-3213-7.

Ghernaout, D., Naceur, M.W., Aouabed, A., 2011. On the dependence of chlorine by-products generated species formation of the electrode material and applied charge during electrochemical water treatment. Desalination 270 (1), 9–22. https://doi.org/10.1016/j.desal.2011.01.010.

Giannakis, S., Voumard, M., Rtimi, S., Pulgarin, C., 2018. Bacterial disinfection by the photo-Fenton process: extracellular oxidation or intracellular photo-catalysis? Appl. Catal. B Environ. 227, 285–295. https://doi.org/10.1016/j.apcatb.2018.01.044.

Gray, H.E., Powell, T., Choi, S., Smith, D.S., Parker, W.J., 2020. Organic phosphorus removal using an integrated advanced oxidation-ultrafiltration process. Water Res. 182, 115968. https://doi.org/10.1016/j.watres.2020.115968.

Halder, S., Yadav, K.K., Sarkar, R., Mukherjee, S., Saha, P., Haldar, S., Karmakar, S., Sen, T., 2015. Alteration of Zeta potential and membrane permeability in bacteria: a study with cationic agents. SpringerPlus 4. https://doi.org/10.1186/s40064-015-1476-7.

Hao, X., Wei, Y., Honghui, Y., 2015. Surface analysis of Ti/Sb-SnO2/PbO2 electrode after long time electrolysis. Rare Met. Mater. Eng. 44 (11), 2637–2641. https://doi.org/10.1016/S1875-5372(16)60009-7.

He, X., Yang, D.-P., Zhang, X., Liu, M., Kang, Z., Lin, C., Jia, N., Luque, R., 2019. Waste eggshell membrane-templated CuO-ZnO nanocomposites with enhanced adsorption, catalysis and antibacterial properties for water purification. Chem. Eng. J. 369, 621–633. https://doi.org/10.1016/j.cej.2019.03.047.

Hirakawa, K., Mori, M., Yoshida, M., Oikawa, S., Kawanishi, S., 2004. Photo-irradiated titanium dioxide catalyzes site specific DNA damage via generation of hydrogen peroxide. Free Radic. Res. 38 (5), 439–447. https://doi.org/10.1080/10715760420002064487.

Holade, Y., Engel, A.B., Servat, K., Napporn, T.W., Morais, C., Tingry, S., Cornu, D., Kokoh, K.B., 2018. Electrocatalytic and electroanalytic investigation of carbohydrates oxidation on gold-based nanocatalysts in alkaline and neutral pHs. J. Electrochem. Soc. 165 (9), H425–H436. https://doi.org/10.1149/2.0311809jes.

Imamura, H., Sakamoto, S., Yoshida, T., Matsui, Y., Penuela, S., Laird, D.W., Mizukami, S., Kikuchi, K., Kakizuka, A., 2020. Single-cell dynamics of pannexin-1-facilitated programmed ATP loss during apoptosis. Elife 9, e61960. https://doi.org/10.7554/eLife.61960.

IS-10500, 2012. Indian Standard Drinking Water–Specification (Second Revision). Bureau of Indian Standards (BIS), New Delhi.

Isidro, J., Brackemeyer, D., Sáez, C., Llanos, J., Lobato, J., Cañizares, P., Matthée, T., Rodrigo, M.A., 2020. Electro-disinfection with BDD-electrodes featuring PEM technology. Separ. Purif. Technol. 248, 117081. https://doi.org/10.1016/j.seppur.2020.117081.

Jasper, J.T., Yang, Y., Hoffmann, M.R., 2017. Toxic byproduct formation during electrochemical treatment of latrine wastewater. Environ. Sci. Technol. 51 (12), 7111–7119. https://doi.org/10.1021/acs.est.7b01002.

Jeong, J., Kim, J.Y., Yoon, J., 2006. The role of reactive oxygen species in the electrochemical inactivation of microorganisms. Environ. Sci. Technol. 40 (19), 6117–6122. https://doi.org/10.1021/es0604313.

Jiang, Y., Zhao, H., Liang, J., Yue, L., Li, T., Luo, Y., Liu, Q., Lu, S., Asiri, A.M., Gong, Z., Sun, X., 2021. Anodic oxidation for the degradation of organic pollutants: anode materials, operating conditions and mechanisms. A mini review. Electrochem. Commun. 123, 106912. https://doi.org/10.1016/j.elecom.2020.106912.

Jin, Y., Shi, Y., Chen, R., Chen, X., Zheng, X., Liu, Y., 2019. Electrochemical disinfection using a modified reticulated vitreous carbon cathode for drinking water treatment. Chemosphere 215, 380–387. https://doi.org/10.1016/j.chemosphere.2018.10.057.

Jin, Y., Wang, Y., Huang, Q., Zhu, L., Cui, Y., Cui, L., 2016. The performance and applicability study of a fixed photovoltaic-solar water disinfection system. Energy Convers. Manag. 123, 549–558. https://doi.org/10.1016/j.enconman.2016.06.073.

Kłodzińska, E., Szumski, M., Dziubakiewicz, E., Hrynkiewicz, K., Skwarek, E., Janusz, W., Buszewski, B., 2010. Effect of zeta potential value on bacterial behavior during electrophoretic separation. Electrophoresis 31 (9), 1590–1596. https://doi.org/10.1002/elps.200900559.

Kourdali, S., Badis, A., Boucherit, A., Boudjema, K., Saiba, A., 2018. Electrochemical disinfection of bacterial contamination: effectiveness and modeling study of E. coli inactivation by electro-Fenton, electro-peroxi-coagulation and electrocoagulation. J. Environ. Manag. 226, 106–119. https://doi.org/10.1016/j.jenvman.2018.08.038.

Lacasa, E., Tsolaki, E., Sbokou, Z., Rodrigo, M.A., Mantzavinos, D., Diamadopoulos, E., 2013. Electrochemical disinfection of simulated ballast water on conductive diamond electrodes. Chem. Eng. J. 223, 516–523. https://doi.org/10.1016/j.cej.2013.03.003.

Lee, H., Jin, Y., Hong, S., 2018. Understanding possible underlying mechanism in declining germicidal efficiency of UV-LED reactor. J. Photochem. Photobiol. B Biol. 185, 136–142. https://doi.org/10.1016/j.jphotobiol.2018.06.001.

Li, H., Zhu, X., Ni, J., 2010. Inactivation of Escherichia coli in Na2SO4 electrolyte using boron-doped diamond anode. Electrochim. Acta 56 (1), 448–453. https://doi.org/10.1016/j.electacta.2010.08.055.

Libardo, M.D.J., Wang, T.-Y., Pellois, J.-P., Angeles-Boza, A.M., 2017. How does membrane oxidation affect cell delivery and cell killing? Trends Biotechnol. 35 (8), 686–690. https://doi.org/10.1016/j.tibtech.2017.03.015.

Lin, H., Niu, J., Ding, S., Zhang, L., 2012. Electrochemical degradation of perfluorooctanoic acid (PFOA) by Ti/SnO2-Sb, Ti/SnO2-Sb/PbO2 and Ti/SnO2-Sb/MnO2 anodes. Water Res. 46 (7), 2281–2289. https://doi.org/10.1016/j.watres.2012.01.053.

Long, Y., Ni, J., Wang, Z., 2015. Subcellular mechanism of Escherichia coli inactivation during electrochemical disinfection with boron-doped diamond anode: a comparative study of three electrolytes. Water Res. 84, 198–206. https://doi.org/10.1016/j.watres.2015.07.035.

Martínez-Huitle, C.A., Rodrigo, M.A., Sirés, I., Scialdone, O., 2015. Single and coupled electrochemical processes and reactors for the abatement of organic water pollutants: a critical review. Chem. Rev. 115 (24), 13362–13407. https://doi.org/10.1021/acs.chemrev.5b00361.

Mempin, R., Tran, H., Chen, C., Gong, H., Kim Ho, K., Lu, S., 2013. Release of extracellular ATP by bacteria during growth. BMC Microbiol. 13 (1), 301. https://doi.org/10.1186/1471-2180-13-301.

Osimani, A., Garofalo, C., Clementi, F., Tavoletti, S., Aquilanti, L., 2014. Bioluminescence ATP monitoring for the routine assessment of food contact surface cleanliness in a university canteen. Int. J. Environ. Res. Publ. Health 11 (10), 10824–10837. https://doi.org/10.3390/ijerph111010824.

Panizza, M., Cerisola, G., 2009. Direct and mediated anodic oxidation of organic pollutants. Chem. Rev. 109 (12), 6541–6569. https://doi.org/10.1021/cr9001319.

Patra, S., Munichandraiah, N., 2009. Electrochemical reduction of hydrogen peroxide on stainless steel. J. Chem. Sci. 121 (5), 675–683. https://doi.org/10.1007/s12039-009-0081-0.

Pei, J., Hsu, C.-C., Yu, K., Wang, Y., Huang, G., 2018. Time-resolved method to distinguish protein/peptide oxidation during electrospray ionization mass spectrometry. Anal. Chim. Acta 1011, 59–67. https://doi.org/10.1016/j.aca.2018.01.025.

Pei, J., Zhou, X., Wang, X., Huang, G., 2015. Alleviation of electrochemical oxidation for peptides and proteins in electrospray ionization: obtaining more accurate mass

spectra with induced high voltage. Anal. Chem. 87 (5), 2727–2733. https://doi.org/10.1021/ac503990a.
Pillet, F., Formosa-Dague, C., Baaziz, H., Dague, E., Rols, M.-P., 2016. Cell wall as a target for bacteria inactivation by pulsed electric fields. Sci. Rep. 6 https://doi.org/10.1038/srep19778.
Pistelok, F., Pohl, A., Stuczyński, T., Wiera, B., 2016. Using ATP tests for assessment of hygiene risks. Ecol. Chem. Eng. S 23 (2), 259–270. https://doi.org/10.1515/eces-2016-0018.
Rahmani, A.R., Samarghandi, M.R., Nematollahi, D., Zamani, F., 2019. A comprehensive study of electrochemical disinfection of water using direct and indirect oxidation processes. J. Environ. Chem. Eng. 7 (1), 102785. https://doi.org/10.1016/j.jece.2018.11.030.
Rajasekhar, B., Nambi, I.M., Govindarajan, S.K., 2021. Investigating the degradation of nC12 to nC23 alkanes and PAHs in petroleum- contaminated water by electrochemical advanced oxidation process using an inexpensive Ti/Sb-SnO2/PbO2 anode. Chem. Eng. J. 404, 125268. https://doi.org/10.1016/j.cej.2020.125268.
Rajasekhar, B., Venkateshwaran, U., Durairaj, N., Divyapriya, G., Nambi, I.M., Joseph, A., 2020. Comprehensive treatment of urban wastewaters using electrochemical advanced oxidation process. J. Environ. Manag. 266, 110469. https://doi.org/10.1016/j.jenvman.2020.110469.
Reipa, V., Atha, D.H., Coskun, S.H., Sims, C.M., Nelson, B.C., 2018. Controlled potential electro-oxidation of genomic DNA. PLoS One 13 (1), e0190907. https://doi.org/10.1371/journal.pone.0190907.
Sanna, T., Dallolio, L., Raggi, A., Mazzetti, M., Lorusso, G., Zanni, A., Farruggia, P., Leoni, E., 2018. ATP bioluminescence assay for evaluating cleaning practices in operating theatres: applicability and limitations. BMC Infect. Dis. 18 (1), 583. https://doi.org/10.1186/s12879-018-3505-y.
Sharma, P., Jha, A.B., Dubey, R.S., Pessarakli, M., 2012. Reactive oxygen species, oxidative damage, and antioxidative defense mechanism in plants under stressful conditions. J. Botany, e217037. https://doi.org/10.1155/2012/217037.
Singh, R.K., Philip, L., Ramanujam, S., 2016. Disinfection of water by pulsed power technique: a mechanistic perspective. RSC Adv. 6 (15), 11980–11990. https://doi.org/10.1039/C5RA26941E.
Sirés, I., Brillas, E., Oturan, M.A., Rodrigo, M.A., Panizza, M., 2014. Electrochemical advanced oxidation processes: today and tomorrow. A review. Environ. Sci. Pollut. Control Ser. 21 (14), 8336–8367. https://doi.org/10.1007/s11356-014-2783-1.
Stalcup, A.M., 2006. Chapter 8—chiral separations by capillary electrophoresis. In: Busch, K.W., Busch, M.A. (Eds.), Chiral Analysis. Elsevier, pp. 241–275. https://doi.org/10.1016/B978-044451669-5/50008-9.
Sun, G., Jia, S., Zhang, X., Kang, Z., Cui, M., Wang, B., Wang, B., Yang, D.-P., 2021. Anchoring core–shell Cu@Cu2O nanoparticles to two-dimensional carbon nanosheets for bacterial disinfection. ACS Appl. Nano Mater. 4 (9), 9831–9841. https://doi.org/10.1021/acsanm.1c02233.
Sun, H., Li, G., Nie, X., Shi, H., Wong, P.-K., Zhao, H., An, T., 2014. Systematic approach to in-depth understanding of photoelectrocatalytic bacterial inactivation mechanisms by tracking the decomposed building blocks. Environ. Sci. Technol. 48 (16), 9412–9419. https://doi.org/10.1021/es502471h.
Tai, C., Peng, J.-F., Liu, J.-F., Jiang, G.-B., Zou, H., 2004. Determination of hydroxyl radicals in advanced oxidation processes with dimethyl sulfoxide trapping and liquid chromatography. Anal. Chim. Acta 527 (1), 73–80. https://doi.org/10.1016/j.aca.2004.08.019.
Taylor, A.A., Chowdhury, I., Gong, A.S., Cwiertny, D.M., Walker, S.L., 2014. Deposition and disinfection of Escherichia coli O157:H7 on naturally occurring photoactive materials in a parallel plate chamber. Environ. Sci. Process. Impacts 16 (2), 194–202. https://doi.org/10.1039/c3em00527e.
Thostenson, J.O., Mourouvin, R., Hawkins, B.T., Ngaboyamahina, E., Sellgren, K.L., Parker, C.B., Deshusses, M.A., Stoner, B.R., Glass, J.T., 2018. Improved blackwater disinfection using potentiodynamic methods with oxidized boron-doped diamond electrodes. Water Res. 140, 191–199. https://doi.org/10.1016/j.watres.2018.04.022.
Tripathy, B.K., Kumar, S., Kumar, M., Debnath, A., 2020. Microwave induced catalytic treatment of brilliant green dye with carbon doped zinc oxide nanoparticles: central composite design, toxicity assessment and cost analysis. Environ. Nanotechnol. Monitor. Manag. 14, 100361. https://doi.org/10.1016/j.enmm.2020.100361.
Velichenko, A.B., Amadelli, R., Benedetti, A., Girenko, D.V., Kovalyov, S.V., Danilov, F.I., 2002. Electrosynthesis and physicochemical properties of PbO2 films. J. Electrochem. Soc. 149 (9), C445. https://doi.org/10.1149/1.1495498.
Weng, M., Yu, X., 2019. Electrochemical oxidation of para-aminophenol with rare earth doped lead dioxide electrodes: kinetics modeling and mechanism. Front. Chem. 7 https://doi.org/10.3389/fchem.2019.00382.
Who, 2017. WHO Guidelines for Drinking Water Quality: First Addenum to the, fourth ed. World Health Organisation.
Xia, Y., Wang, G., Guo, L., Dai, Q., Ma, X., 2019. Electrochemical oxidation of Acid Orange 7 azo dye using a PbO2 electrode: parameter optimization, reaction mechanism and toxicity evaluation. Chemosphere 241, 125010. https://doi.org/10.1016/j.chemosphere.2019.125010.
Xue, B., Zhang, Y., Wang, J.Y., 2011. Electrochemical oxidation of bisphenol A on Ti/SnO2- Sb2O5/PbO2 anode for waste water treatment. Procedia Environ. Sci. 10, 647–652. https://doi.org/10.1016/j.proenv.2011.09.104.
Yang, Y., Xia, Y., Wei, F., Zhang, L., Yao, Y., 2020. Electrochemical oxidation of the pesticide nitenpyram using a Gd-PbO2 anode: operation parameter optimization and degradation mechanism. J. Chem. Technol. Biotechnol. 95 (8), 2120–2128. https://doi.org/10.1002/jctb.6397.
Yuan, M., Salman, N.M., Guo, H., Xu, Z., Xu, H., Yan, W., Liao, Z., Wang, Y., 2019. A 2.5D electrode system constructed of magnetic Sb–SnO2 particles and a PbO2 electrode and its electrocatalysis application on acid red G degradation. Catalysts 9 (11), 875. https://doi.org/10.3390/catal9110875.
Zeng, X., Lan, S., Lo, I.M.C., 2019. Rapid disinfection of E. coli by a ternary BiVO4/Ag/g-C3N4 composite under visible light: photocatalytic mechanism and performance investigation in authentic sewage. Environ. Sci.: Nano 6 (2), 610–623. https://doi.org/10.1039/C8EN01283K.
Zhang, C., Li, Y., Wang, C., Zheng, X., 2021. Different inactivation behaviors and mechanisms of representative pathogens (Escherichia coli bacteria, human adenoviruses and Bacillus subtilis spores) in g-C3N4-based metal-free visible-light-enabled photocatalytic disinfection. Sci. Total Environ. 755, 142588. https://doi.org/10.1016/j.scitotenv.2020.142588.
Zhang, M., Dong, H., Zhao, L., Wang, D., Meng, D., 2019a. A review on Fenton process for organic wastewater treatment based on optimization perspective. Sci. Total Environ. 670, 110–121. https://doi.org/10.1016/j.scitotenv.2019.03.180.
Zhang, X., He, X., Kang, Z., Cui, M., Yang, D.-P., Luque, R., 2019b. Waste eggshell-derived dual-functional CuO/ZnO/eggshell nanocomposites: (Photo)catalytic reduction and bacterial inactivation. ACS Sustain. Chem. Eng. 7 (18), 15762–15771. https://doi.org/10.1021/acssuschemeng.9b04083.